Control Allocation Reconfiguration for Actuator Failure on a Coaxial-Pusher Helicopter

Michael E. McKay *
Ph.D. Graduate

Praneet Vayalali
Ph.D. Graduate

Farhan Gandhi
Redfern Chair Professor, Director

Center for Mobility with Vertical Lift, Rensselaer Polytechnic Institute Troy, NY

Tom Berger
Flight Controls Group Lead

Mark J. S. Lopez
Flight Dynamics Modeling SME

U.S. Army Combat Capabilities Development Command Aviation & Missile Center, Moffet Field, CA

An elastic blade flight dynamics model for a coaxial helicopter platform based on the Sikorsky X2 Technology™ Demonstrator is presented and validated with steady trim and frequency response flight-test data. A full authority explicit model following control architecture along with pseudoinverse control allocation is implemented for the model in hover and cruise at 180 kt using CONDUIT® in order to stabilize the vehicle and meet a set of stability, handling qualities, and performance requirements. Different fault scenarios are considered including failure of rotor swashplate actuators and tail surface actuators in hover and forward flight, which are compensated for by recalculating the pseudoinverse control mixing accordingly. The approach is shown to maintain aircraft stability through the fault transient and into a new steady trim state for the vehicle. Though the implemented controller is successful in maintaining the aircraft state, different fault cases lead to violations in rotor tip clearance limits, which will require additional effort to account for in flight.

Nomenclature

n_z	stability axis vertical acceleration, g
s_{aft}	aft swashplate actuator position, %
s_{lat}	lateral swashplate actuator position, %
s_{fwd}	forward swashplate actuator position, %
δ_{lat}	lateral mixer input, deg/s^2
δ_{lon}	longitudinal mixer input, deg/s^2
p	body frame roll rate, deg/s
q	body frame pitch rate, deg/s
Γ	swashplate control phase angle, deg
$\Delta\theta_{\text{lat}}$	differential lateral pitch, deg
$\Delta\theta_{\text{lon}}$	differential longitudinal pitch, deg
$\Delta\theta_0$	differential collective pitch, deg
δ_e	elevator deflection (deg), positive TE down
δ_r	rudder deflection (deg), positive TE left
θ_0	symmetric collective pitch, deg
θ_{lon}	symmetric longitudinal pitch, deg
θ_{lat}	symmetric lateral pitch, deg

*Corresponding author; email: michael.mckay005@gmail.com.
Presented in the Advanced Vertical Flight Session of the Vertical Flight Society 77th Annual Forum & Technology Display, Virtual, May 10–14, 2021. Manuscript received February 2022; accepted October 2022.
Distribution Statement A: Approved for public release.

Introduction

High-speed coaxial helicopters are poised to revolutionize the future of vertical flight. The ability of this aircraft type to perform typical Vertical Takeoff and Landing (VTOL) missions as well as push the flight envelope and mission capabilities into a high-speed regime is a feat rotary wing vehicles have traditionally been unable to perform. With the establishment of the Department of Defense's Future Vertical Lift (FVL) initiative (Ref. 1), coaxial-pusher helicopters have become an area of recent interest. This nontraditional VTOL aircraft has the ability

to fly farther, faster, and longer than the current fleet of conventional (single main rotor) rotorcraft being utilized. Under the Joint Multi-Role Technology Demonstrator program, these vehicles are being built and tested in order to study and improve these future concepts.

A unique feature of these aircraft, as well as other advanced rotorcraft concepts, is the availability of multiple redundant effectors typically not present on legacy rotary wing vehicles. These enable the aircraft to achieve nonunique trim states that can be varied depending on the objective of the mission or in order to compensate for a component failure in the other flight controls. In recent work, the ability to utilize redundant controls for power minimization, load alleviation, and noise reduction has been explored on different FVL-type platforms. Different studies performed at Rensselaer Polytechnic Institute (RPI) have considered power and vibration reduction using redundant controls on the XH-59A coaxial helicopter (Ref. 2) and a compounded UH-60 Black Hawk (Refs. 3, 4). Additional work has been performed at the University of Maryland for optimal multiobjective trim on the generic coaxial platform (Refs. 5–7), considering performance, loads, and noise.

Outside of trim simulations, there has also been substantial effort made to develop flight simulation models of coaxial-pusher aircraft for flight control design and handling qualities evaluation. These studies range from the development of generic models (Ref. 8) to the development and improvement of specific models of the X2 Technology™ Demonstrator (X2TD) in a collaborative effort between the U.S. Army and Sikorsky (Refs. 9, 10). In addition to the modeling effort, significant work has gone into inner and outer loop flight control design for high-speed vehicles, including coaxial helicopters (Refs. 11, 12) outside of the internal development undertaken during production and flight testing of the FVL candidates. These studies highlight the specific challenges (stability, tip clearance, response types) present in the control design of coaxial helicopter platforms and provide potential approaches to achieve good handling qualities performance.

Recently, work at RPI has investigated the use of redundant controls for fault compensation after an actuator lock in the swashplate of a compound helicopter in trim (Ref. 13) and in dynamic simulation (Refs. 14, 15). Previously, work at RPI demonstrated the ability to compensate for flight control failure on the UH-60A (Refs. 16, 17), demonstrating that the extra controls present can allow for recovery and steady-level flight after a component failure in certain flight conditions. In addition to this body of work, the U.S. Army and Piasecki have published a study considering damage tolerant control on the Piasecki X-49A (Ref. 18), where multiple control allocation techniques were implemented and compared in different fault scenarios in piloted simulation.

There is no substantial body of work investigating the use of redundant control effectors to compensate for component failure in different flight conditions for a lift-offset coaxial-pusher helicopter. The present study seeks to build off of prior publication by the authors (Ref. 19), where the ability of a coaxial helicopter to trim postcontrol failure was investigated and examine the potential use of redundant control allocation to compensate for failure in the available flight controls, considering the method of control allocation and potential fault cases where a redefinition of the allocation can allow for safe recovery of the vehicle.

Flight Dynamics Model

Simulation results are obtained from the RPI Coaxial Helicopter Analysis and Dynamics (CHAD) code. The code utilizes a blade element theory model coupled with a pressure potential superposition inflow model (Ref. 20) to calculate rotor forces and moments for a given operating condition and control input. This rotor model has been presented and validated in prior publication by the authors (Ref. 19) against coaxial rotor test data from NACA (Ref. 21) and UT Austin (Ref. 22). The aircraft fuselage and control surfaces are modeled according to the published XV-15 simulation model (Ref. 23), with appropriate scaling to represent the vehicle being considered, which is the X2TD in the present study. Finally, the pusher propeller is modeled with momentum theory with appropriate consideration for nonideal losses in order to match published flight-test data. Overall, the CHAD bare-airframe model has a total of 50 states: 12 rigid body, 32 rotor (2 states per mode × 2 blade modes × 4 blades × 2 rotors), and 6 main rotor inflow (3 states per rotor). Model validation has been performed for trim controls, performance, and identified flight dynamics data taken from flight test of the X2TD. The CHAD model compares well to flight-test data as well as other established comprehensive codes; full model validation and discussion can be found in Refs. 24 and 25.

Table 1. Coaxial rotor controls

Control	Description
θ_0	Symmetric collective
θ_{lon}	Symmetric longitudinal
θ_{lat}	Symmetric lateral
$\Delta\theta_0$	Differential collective
$\Delta\theta_{lon}$	Differential longitudinal
$\Delta\theta_{lat}$	Differential lateral

Rotor controls and swashplate representation

The full set of coaxial rotor head controls is given in Table 1. For the present study, swashplate actuators are assumed to be located at $-\Gamma$, $90^\circ-\Gamma$, and $180^\circ-\Gamma$ in the appropriate swashplate azimuthal coordinate. Note that this placement is a typical geometry, but the position of the actuators can have a notable impact on survivability in fault cases. Future work should consider the sensitivity of these positions and potentially optimize actuator positions for damage tolerance. These actuators are consequently labeled s_{aft}, s_{lat}, and s_{fwd} for each rotor. The results that follow assume an allowable collective setting range from −5 to 15 deg on each rotor, which results in a $\pm 10^\circ$ range in θ_{1c} and $\pm 20^\circ$ in θ_{1s} according to the swashplate model developed and detailed in Refs. 24 and 25.

Control Architecture

Linearized aircraft models are extracted from CHAD in hover and cruise and are stabilized and controlled with an explicit model following (EMF) control architecture. This design is chosen for its wide use in modern aircraft control problems as well as the ease of independently tuning performance and disturbance rejection characteristics. A basic overview of the control system is given in Fig. 1. Two flight conditions are considered, hover and 180 kt, and different response types are designed for each case, outlined in Table 2. The control system is designed similar to the architecture designed for the U.S. Army generic coaxial model, presented in Ref. 11, with the exception of a forward path tip clearance controller.

The design parameters of the control system are optimized with the Control Designer's Unified Interface, CONDUIT® (Ref. 26). This software optimizes the feedback gains in the system to meet a set of stability, handling qualities, and performance specifications, listed in Table 3. Note that in cruise, the stability margin requirement in pitch had to be relaxed (to 3 dB and 23°) due to the bare airframe dynamics at this condition, this was also done for the U.S. Army generic coaxial model in Ref. 11

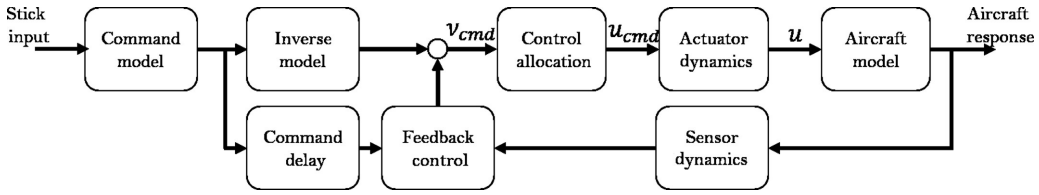

Fig. 1. EMF block diagram.

Table 2. Response type summary

Axis	Hover	180 kt
Lateral	RCAH	RCAH
Longitudinal	RCAH	n_z command/α hold
Directional	RC DH	β command/TC
Vertical	RCHH	Direct Stick to head

Table 3. CONDUIT specifications

Specification	Axis
Stability requirements	
Eigenvalue stability	All
Stability margins	All
Nichols margins	All
Handling qualities requirements	
Eigenvalue damping	All
Model following cost	All
Bandwidth and time delay	Roll/pitch/yaw
Heave response	H
Disturbance rejection bandwidth/peak	All
Open loop onset point	All
Minimum crossover	All
Performance requirements	
Crossover frequency	All
Actuator RMS	All

above 260 kt. These stability margins are not necessarily representative of the actual X2TD, but given the quality of validation between the model and flight-test data (shown in Ref. 24), this indicates a limitation of the control system. A more detailed description of the control system design is also available in Ref. 24).

Control allocation

The coaxial helicopter has control redundancy in all nominal operating states, with two rotors that have collective and cyclic pitch control, aerosurfaces on the horizontal and vertical stabilizers, and a pusher propeller with minimally collective feathering pitch control (some models include monocyclic for moment generation). This set of controls can be represented by

$$\vec{u} = [\theta_0 \;\; \theta_{\text{lon}} \; \theta_{\text{lat}} \; \Delta\theta_0 \;\; \Delta\theta_{\text{lon}} \; \Delta\theta_{\text{lat}} \; \delta_e \; \delta_r \; T_{\text{prop}}] \tag{1}$$

With more controls than are required, some type of allocation scheme is necessary to make the best use of all available effectors. The present study utilizes a weighted pseudoinverse control allocation, which solves

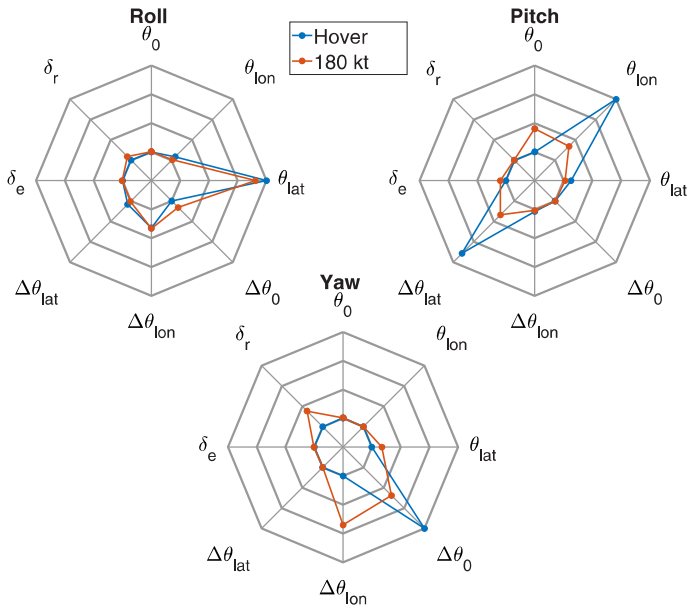

Fig. 2. Control allocation for hover and cruise.

the optimization problem posed as

$$\min ||Wu||_2 \quad s.t. \quad \nu_{\text{cmd}} = Bu \tag{2}$$

$$W_{ii} = \frac{1}{(u_{\max} - u_{\min})} \tag{3}$$

where W is a diagonal weighting matrix defined by the position limits of the available controls (Eq. (3)) and ν_{cmd} is a vector of desired accelerations. The solution to this problem is well known (Refs. 27, 28), and the allocation takes the form

$$u_{\text{cmd}} = M\nu_{\text{cmd}} \qquad M = W^{-1}B^T(BW^{-1}B)^{-1} \tag{4}$$

Note that only the relevant rows of the B matrix are taken in this formulation, which are typically the rows for the angular acceleration ($\dot{p}$, $\dot{q}$, $\dot{r}$) equations of the vehicle dynamic response but could include the vertical acceleration as well if desired. Note that the weighting can be manipulated as desired by the control designer, but typically these weights are defined based on the allowable range of the actuator throw, rate limitations, or some other parameter that reflects the relative limitation of the actuators relative to one another. In the present study, the allocation for lateral, longitudinal, and directional mixer input is given in Fig. 2.

Summarizing the spider plots given in Fig. 2, the roll control mixer appears similar in hover and in cruise, with some small variation in the relative mixing between θ_{lat} and $\Delta\theta_{\text{lon}}$ representing slight changes in the effective control phase angle for the swashplate in this axis. This is expected since there is no aerosurface redundant control in the roll axis

(i.e., no aileron-type effectors). Pitch moment allocation primarily utilizes θ_{lon} and $\Delta\theta_{lat}$ in hover, as is expected because the rotor is the only effective control in this speed. Again, the sharing between symmetric longitudinal (θ_{lon}) and differential lateral ($\Delta\theta_{lat}$) cyclic creates additional effective control phasing in the swashplate, with the variation in this sharing more pronounced in the longitudinal axis. At cruise speeds, the pitch moment allocation utilizes the symmetric collective and elevator deflection as well, due to the increased effectiveness of these inputs at a higher advance ratio. Finally, the yaw moment allocation utilizes only differential collective in hover but utilizes a shared control effort between rudder, differential longitudinal, symmetric lateral, and differential collective control in cruise. Note that additional weighting could be utilized to favor different controls in hover and in cruise (in order to bias effort away from the rotor if desired), but the results presented here simply utilize the pseudoinverse solution weighted by the position limitations of the effectors. A full set of control sensitivities is provided for this vehicle model in Ref. 24.

Nonlinear verification

In order to establish confidence in the linear simulation model used to analyze different flight and fault conditions, a comparison of the linear model predictions and full nonlinear model response is conducted. A subset of the verification is presented here for the lateral and longitudinal broken loop frequency responses in hover and cruise conditions, a full set of results is given in Ref. 24. Figures 3 and 4 give the broken loop frequency response for the lateral and longitudinal axes in hover, as well as Comprehensive Identification from FrEquency Responses (Ref. 29) identified broken loop responses for the nonlinear system. A mismatch cost, J, is calculated between the linear and identified frequency responses based on a weighted magnitude and phase errors squared (Ref. 29). For the responses given in Figs. 3 and 4, the costs are $J = 74.33$ and 40.93, respectively. In cruise, the same axis comparisons give cost values of $J =$ 6.01 and 10.0. The higher cost associated with hover is a result of differences in the low-frequency range around the phugoid mode, as apparent in Figs. 3 and 4. Additional cost comparisons for the remaining broken and closed loop responses are given in Ref. 24. These low-cost values and the qualitative agreement observed in the figures give confidence in the use of the linear model for further analysis.

Control reconfiguration

In the event of actuator failure in any of the available controls, the control laws (command models, inverse models, feedback gains) themselves are not reconfigured, but the control allocation is redefined such that the failed effector is no longer in use. The method is performed assuming fault detection and identification has occurred. To remove the damaged effector from the allocation, the corresponding column in the B matrix used in Eq. (4) is set to zero, and the mixer (M; Eq. (4)) is recomputed similar to the pseudoinverse damage tolerant control method described in Ref. 18. By solving the problem in this manner, the constraint that $\nu_{cmd} = Bu$ is preserved and the newly computed control modes still accomplish the same acceleration commanded by the feedback and feedforward control.

Simulation Results

A selection of linear simulations is performed in hover and cruise at 180 kt. These cases include piloted maneuvers in a healthy aircraft state as well as jammed actuator fault cases during steady-level flight. In both cases, the aircraft performance will be highlighted and discussed in terms of its tracking performance as well as additional considerations including rotor tip clearance and any undesirable vehicle responses, particularly in fault cases.

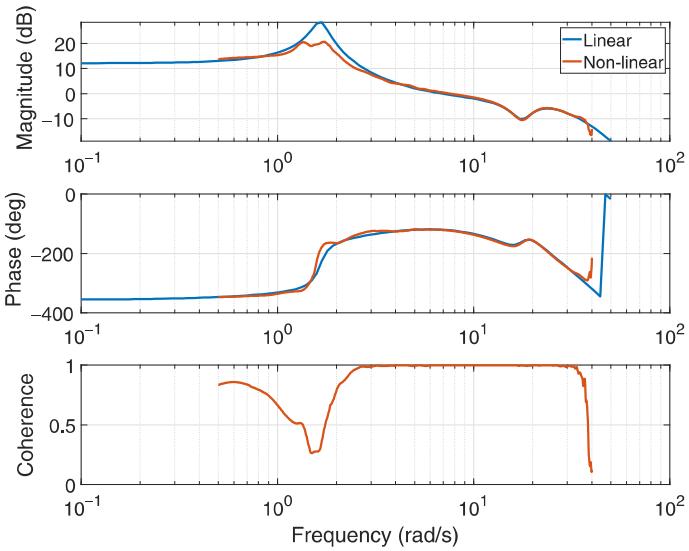

Fig. 3. Lateral broken loop frequency response comparison, hover.

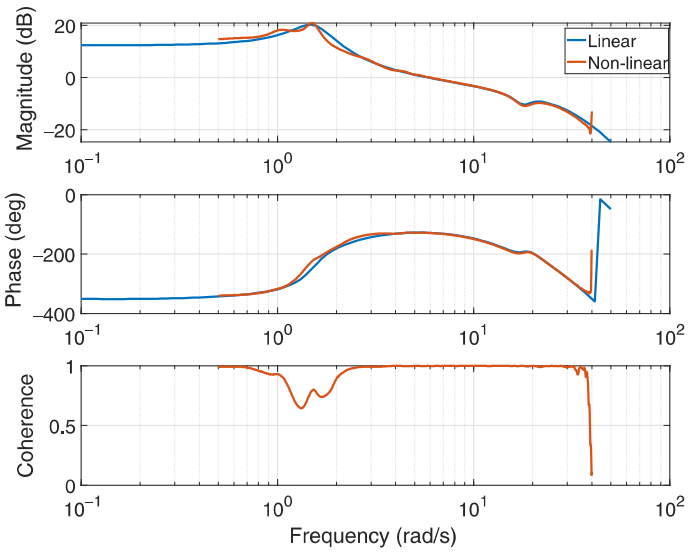

Fig. 4. Longitudinal broken loop frequency response comparison, hover.

Hover baseline responses

In hover, the vehicle response to piloted input is chosen as rate command for all axes (Rate Command Attitude Hold (RCAH) for lateral pitch/roll, Rate Command Direction Hold for yaw, and Rate Command Height Hold for vertical). Note that as stated in Ref. 11, this is sufficient to provide Level 1 handling qualities in a good visual environment. A series of piloted maneuvers are presented in Figs. 5–8 to demonstrate the baseline response characteristics of the closed loop system and to highlight trends in the tip clearance behavior of the vehicle.

Figure 5 depicts the aircraft roll response and tip clearance for a simulated pilot lateral cyclic pulse of 25 deg/s roll rate (50% of required maximum for Level 1 aggressive agility handling qualities requirements;

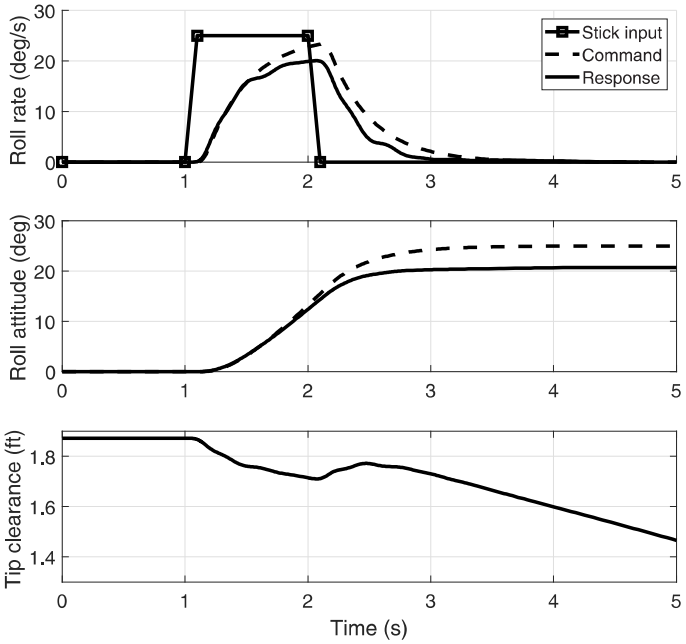

Fig. 5. Lateral cyclic pulse response.

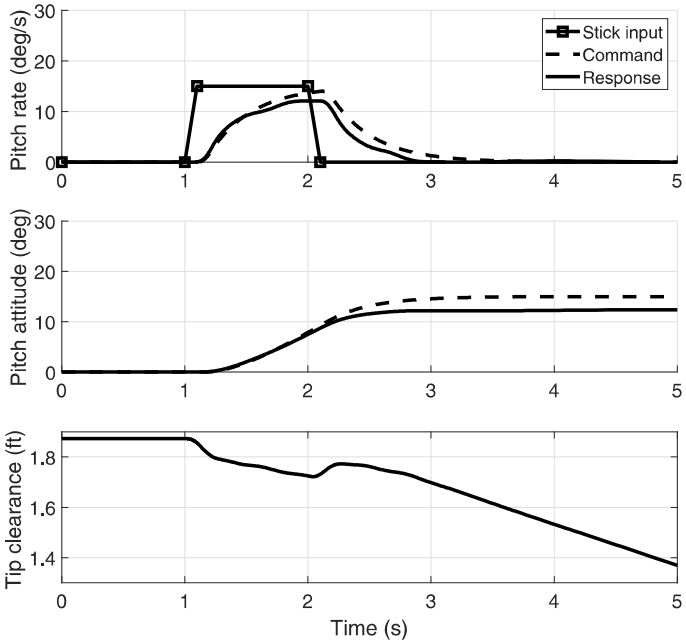

Fig. 6. Longitudinal cyclic pulse response.

(Ref. 30). The roll rate response is nominally first order, and the roll attitude follows a step response with some steady-state error (approximately 4). This steady-state error is expected and caused by the vehicles translation and rotor blowback. Increasing the feedback integral gain can help reduce the steady-state error; however, it comes at the cost of decreased stability margins and increased overshoot. The integral gain value used here was a compromise between these competing requirements. When the maneuver is initiated at 1 s, the rotor tip clearance decreases, then begins to return to the nominal value. Note that the tip clearance does begin to steadily decrease after the stick input ends, which is a result of the vehicle accelerating laterally due to the steady roll attitude and may not be an accurate representation of the vehicle response due to the linear plant dynamics.

Similarly, the pitch response and tip clearance are given for a longitudinal cyclic pulse (15 deg/s command, 50% of required maximum for Level 1 aggressive agility handling qualities requirements (Ref. 30)) in Fig. 6. Again, the vehicle follows a nominal first-order command from the pulse input and settles with a steady-state error in the pitch attitude of approximately 2.7° and the tip clearance drops at the start of the pilot input, and begins to return before entering a steady decline as the vehicle accelerates longitudinally away from the hover condition.

Next, a piloted pedal kick is simulated to demonstrate the baseline system performance in yaw. This rate command response is again first order, where the pilot commands 30 deg/s (50% of required maximum for Level 1 aggressive agility handling qualities requirements (Ref. 30)) of the yaw rate (Fig. 7). The system displays excellent command tracking and virtually zero steady-state error. Generating the torque required to perform such a maneuver, however, requires a differential collective input to the rotor, which results in a differential coning flap response and a significant change in the tip clearance behavior.

Lastly, a collective step is simulated for the system, with a pilot-commanded climb rate of 1500 ft/s. As was the case in the pedal kick, the system exhibits excellent command tracking of the first-order response (Fig. 8). Unlike the pedal kick, however, the thrust required to achieve climb is accomplished with a change in symmetric collective pitch, which has little effect on the rotor tip clearance, and so is not shown here.

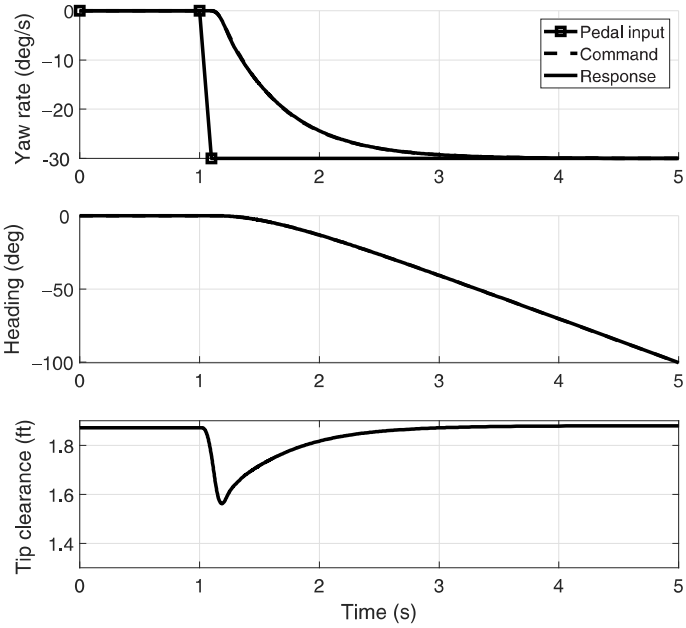

Fig. 7. Pedal kick yaw response.

Hover failure cases

A selection of swashplate actuator locked failures is considered during steady hover in simulation. In all cases, the actuator being considered is locked 15% above the nominal trim position at 5 s. At the same time, the allocator is redefined as described in the Control Reconfiguration section in order to best use the available control set. Because of the symmetry in the hover condition, only two cases are shown here: locked failure of the upper rotor aft and lateral actuators. Note that in the upper actuator failure case, nonlinear simulation results are co-plotted with the linear responses to demonstrate that the linear model considered in most

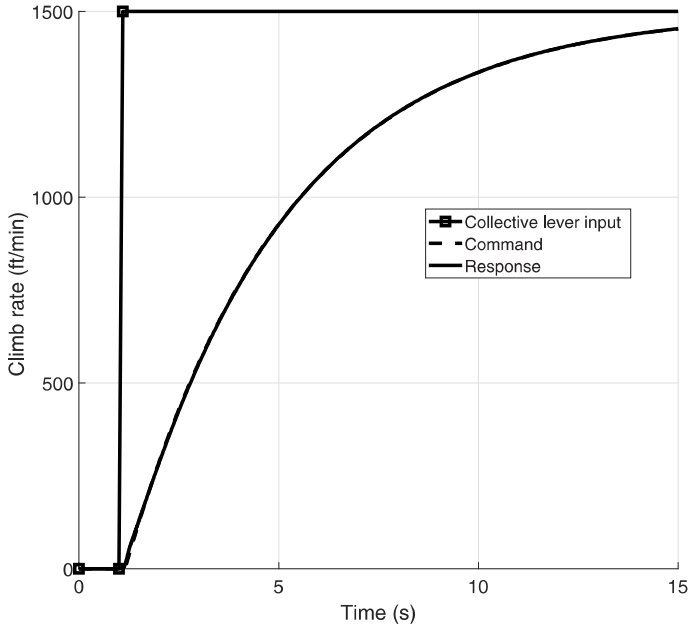

Fig. 8. Collective pull climb response.

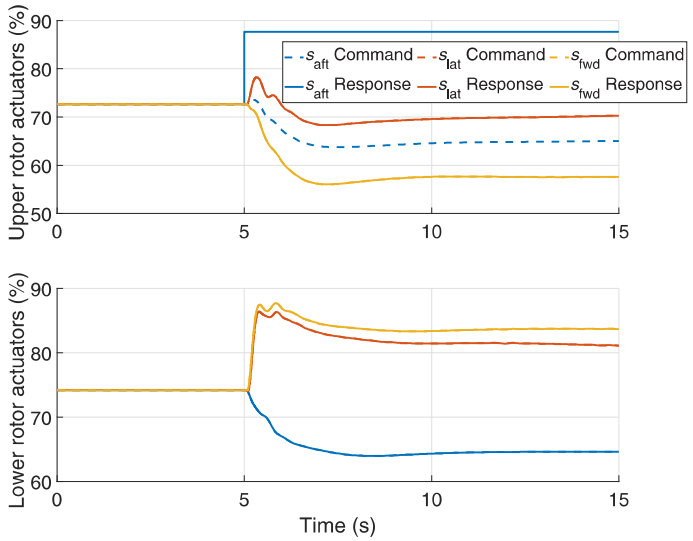

Fig. 9. Upper rotor aft actuator failure actuator positions.

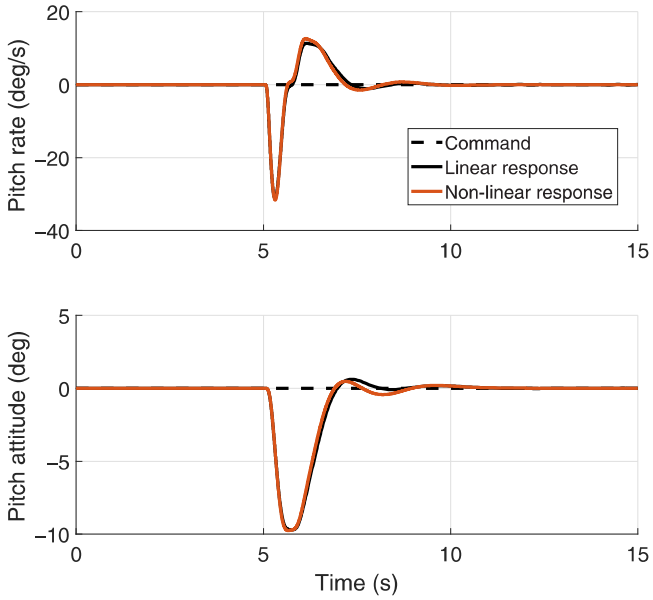

Fig. 10. Upper rotor aft actuator failure pitch response.

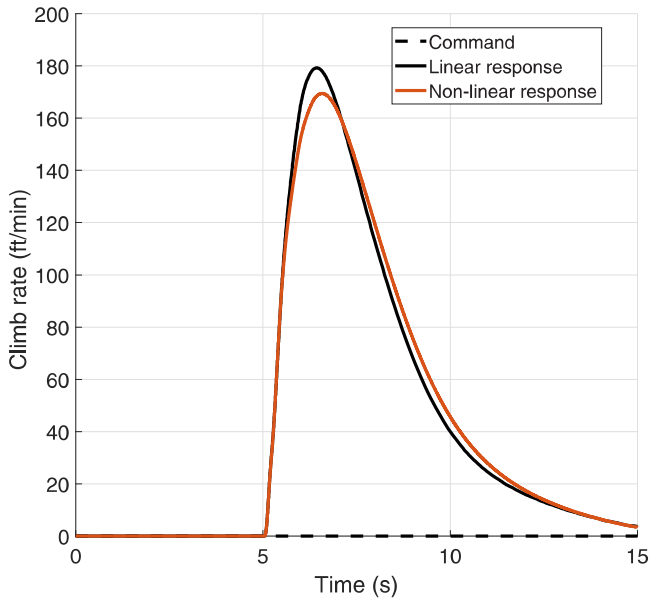

Fig. 11. Upper rotor aft actuator failure climb rate.

conditions accurately represents the full nonlinear vehicle response, even in failure cases.

The aft swashplate actuator is located at $\psi = 0$ in the swashplate azimuth, hence the naming convention chosen. Given this location and the stiffness of the coaxial rotor system, it is expected that displacement of this actuator (Fig. 9) from trim will result in a large nose-down moment coming from the upper rotor as well as an increase in the rotor thrust resulting from the increase in θ_{1c} and θ_0 on the upper rotor. Note that the commanded position of the upper rotor aft actuator (dashed blue line in the top subfigure of Fig. 9) does not remain flat as was suggested in previous discussion. This is simply because only the roll, pitch, and yaw controls are defined by the pseudoinverse allocator, where the collective control is always defined as symmetric collective pitch applied to both rotors, even after failure. Because in hover the rate command, height hold loop is closed, the collective channel is still active and can result in commands being sent to this failed actuator. As depicted by the solid blue line response, however, the failed actuator does not move once the fault has occurred.

In addition to the response in the vehicle motion, the large change in the upper rotor moment and the locked position of the aft actuator will require the lower rotor to generate an equal and opposite pitching moment to compensate and maintain the commanded hover condition, which will greatly impact the rotor tip clearance. The pitch rate and attitude are given in Fig. 10, followed by the climb rate in Fig. 11. Clearly, the system recovers to hover well, with pitch rate settling approximately 3 s after the failure. The deviation in pitch attitude is around 10 deg at maximum, which places the response in Level 2 according to Table III of ADS-33E (Ref. 30), or acceptable for failures that occur less than 2.5×10^{-3} times per flight hour (once per 400 flight hours).

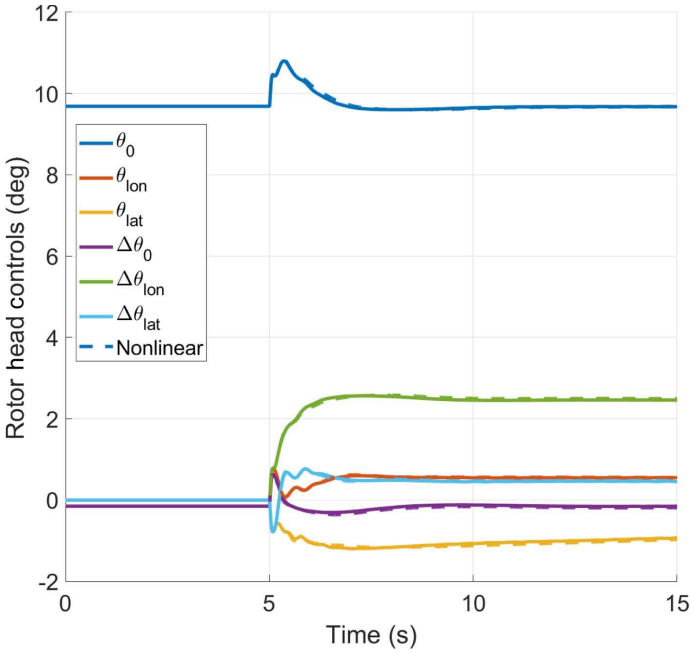

Fig. 12. Upper rotor aft actuator failure rotor head controls.

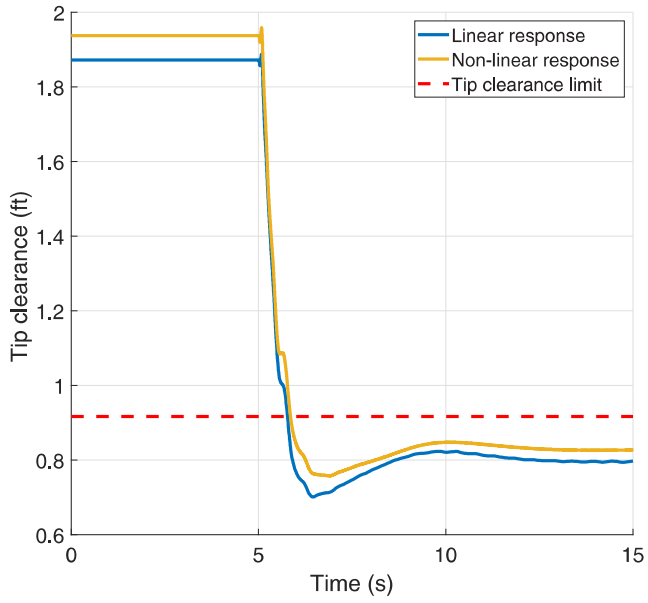

Fig. 13. Upper rotor aft actuator failure tip clearance.

Following from the actuator position time history given in Fig. 9, the resulting rotor head controls are given in Fig. 12. Primary compensation is achieved by a reduction of the lateral and forward actuators on the upper swashplate to reduce the collective pitch, while mirroring the actuator positions on the lower rotor. This mirrored response results in a substantial differential longitudinal cyclic input (green curve in Fig. 12), which leads to a significant differential longitudinal flap response and a reduction in the rotor tip clearance (Fig. 13). Note that this tip clearance violates the flight test observed tip clearance for the X2TD of 11 inches ($\sim$ 0.92 ft) defined in Ref. 31 "to ensure margin during initial envelope expansion." However, this may be acceptable for a failure case as the separation between the rotors is still maintained.

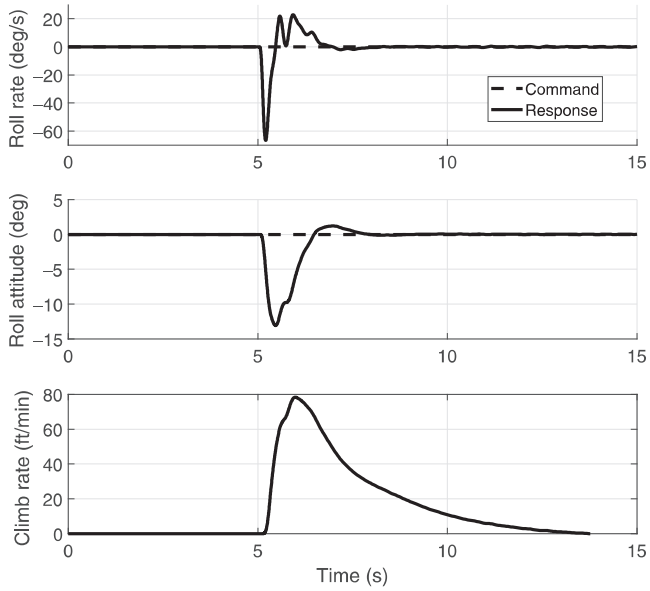

Fig. 14. Upper Rotor lateral actuator failure response.

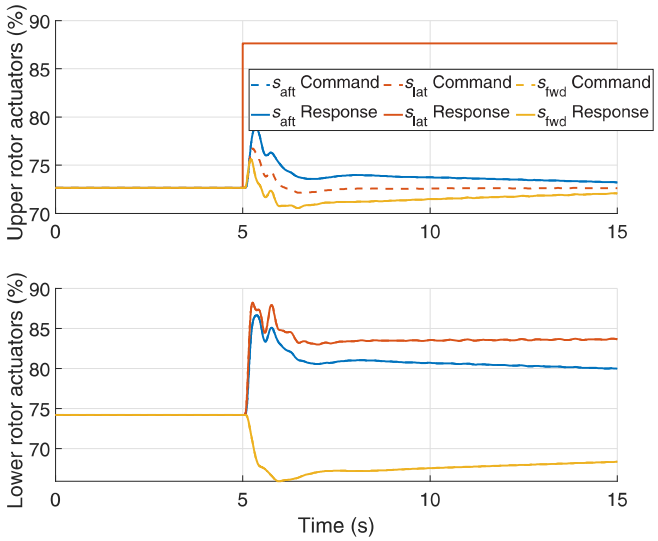

Fig. 15. Upper rotor lateral actuator failure actuator positions.

The lateral actuator failure case is similar to the aft actuator case, except the primary vehicle response comes in the roll axis, because the lateral actuator on the upper rotor swashplate is located at $\psi = 90^\circ$ on the counterclockwise azimuth, so locking above the trim position generates a negative (roll-left) rolling moment. The roll and climb rate responses are shown in Fig. 14. It should be noted that due to the smaller vehicle inertia in roll, the roll attitude that results from the same magnitude failure is larger than the pitch attitude deviation for the aft actuator failure case, yielding a Level 3 failure transient response for this case, which is acceptable for failures that occur less than 2.5×10^{-5} times per flight hour (once per 40,000 flight hours).

Finally, the compensation for the lateral actuator failure (Fig. 15) requires a similar set of rotor head controls (Fig. 16) relative to the aft actuator fault case, but utilization of differential lateral cyclic instead of differential longitudinal due to the lateral actuator fault. However, the rotor tip clearance (Fig. 17) is still reduced in a similar manner through differential lateral flapping.

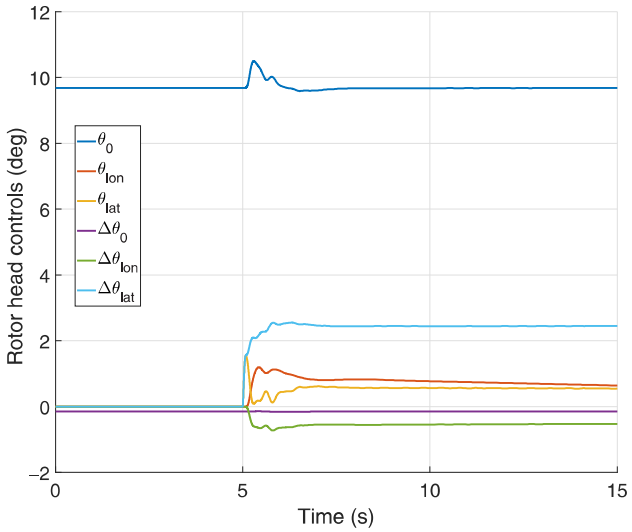

Fig. 16. Upper rotor lateral actuator failure rotor head controls.

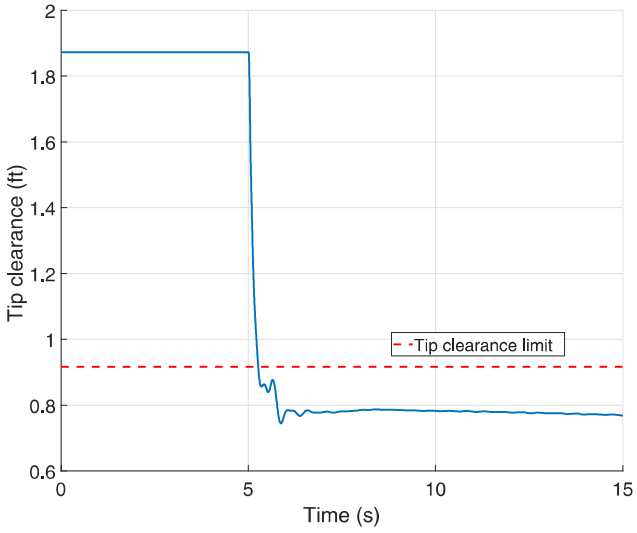

Fig. 17. Upper rotor lateral actuator failure tip clearance.

180 kt baseline response

At 180 kt, the response to pilot input is changed in every control axis except lateral cyclic, which remains RCAH. The longitudinal cyclic now controls stability axis vertical acceleration (n_z) command, angle of attack hold, pedal input controls sideslip command, turn coordination, and the collective lever is now direct stick-to-head control, where the symmetric collective pitch of the rotor system is directly commanded by the collective lever position. The longitudinal stick response changes from rate command to stability axis vertical acceleration (n_z) command in order to stabilize the short period mode present in the plant dynamics. This approach was also taken on the generic coaxial-pusher simulation model developed by the Army (Ref. 11). The pedal response change to sideslip command in cruise allows for automatic turn coordination and is typical for high-speed vehicles. As was done for the hover condition, the baseline stick responses are presented here for reference.

The lateral stick response is very similar to that presented in Fig. 5, with the exception that the commanded rate is larger representing the larger maximum attainable roll rate requirement of 90 deg/s for Level 1

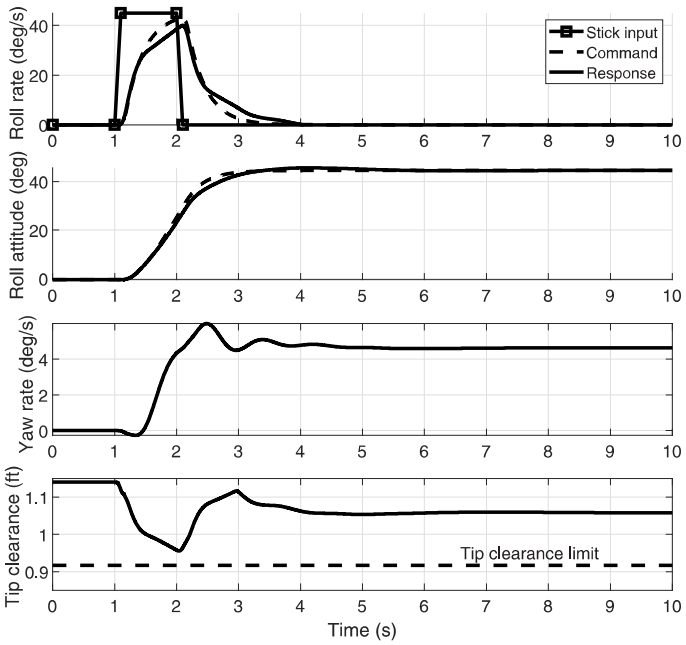

Fig. 18. Lateral cyclic pulse response, cruise.

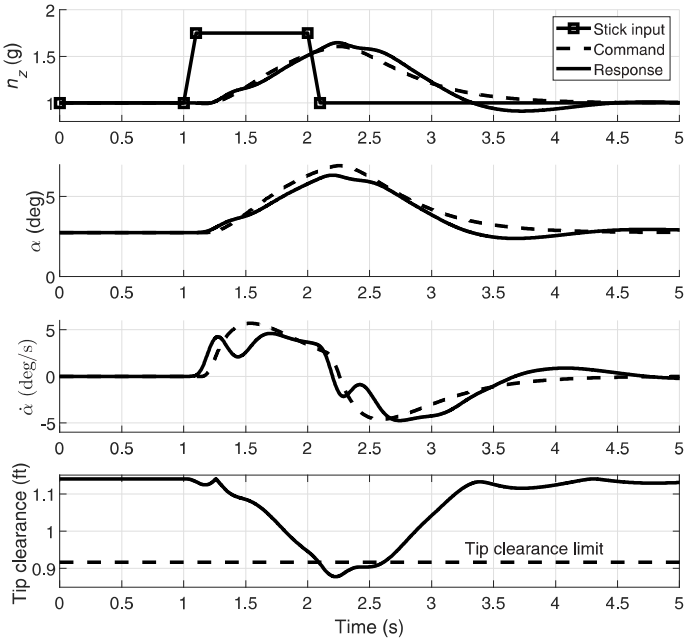

Fig. 19. Longitudinal cyclic pulse response, cruise.

piloted handling qualities in forward flight (the present study provides 50% maximum rate commands for reference). The roll rate, roll attitude, yaw rate, and rotor tip clearance are given in Fig. 18. Note that because of the zero sideslip angle commanded by zero pedal deflection, the vehicle also enters a coordinated turn, indicated by the nonzero steady yaw rate. The tip clearance behavior is characterized by a large initial transient due to the roll acceleration of the vehicle, followed by a steady-state difference from the nominal tip clearance due to some of the rotor controls being used to maintain the coordinated turn.

A baseline response to a 0.75-g pulse command is given in Fig. 19, along with the resultant tip clearance. Note that the primary use of rotor

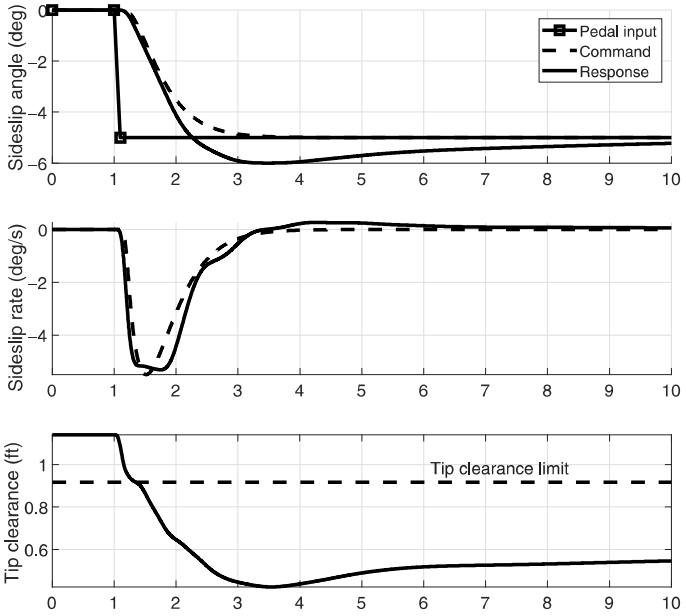

Fig. 20. Pedal kick response, cruise.

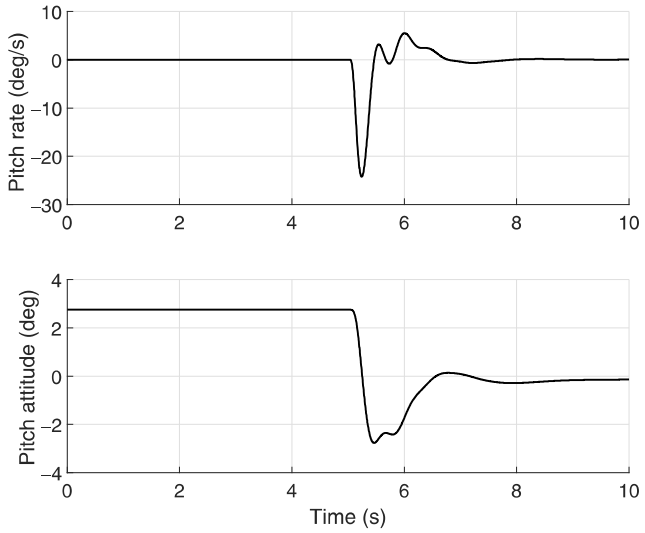

Fig. 21. Elevator failure pitch response, cruise.

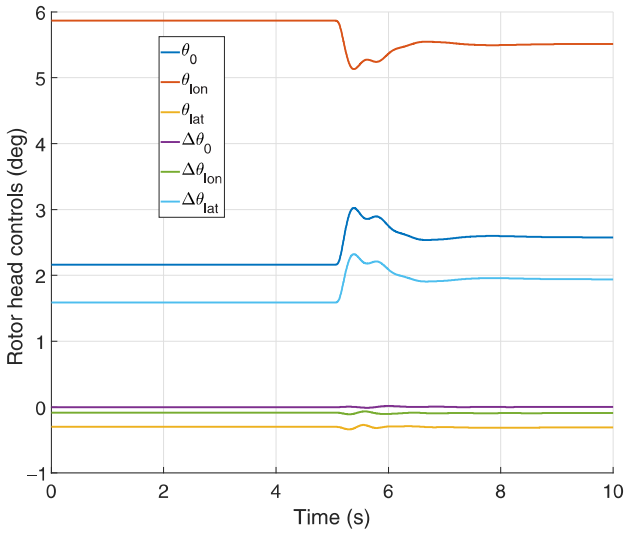

Fig. 22. Elevator failure rotor head controls, cruise.

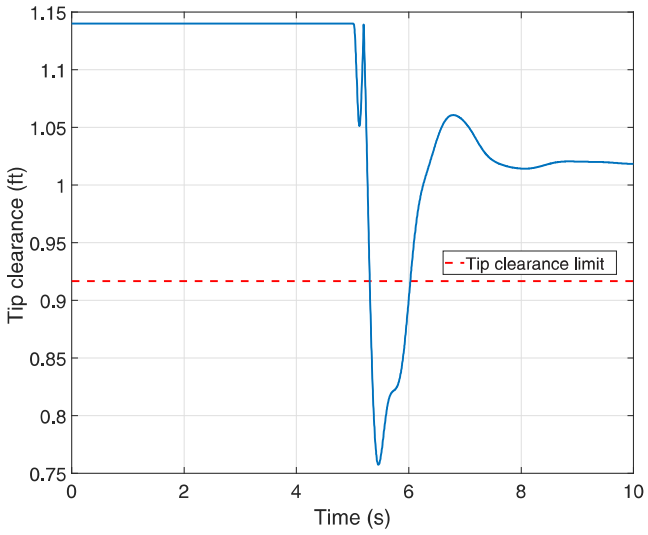

Fig. 23. Elevator failure tip clearance, cruise.

controls IN the pitch allocation results in a large tip clearance response that violates the 11 inches (0.92 ft) clearance limit. This suggests that a more careful design of the weights in the allocation should be considered to utilize the elevator more heavily.

The response to pedal input is given in Fig. 20. Note that the control allocation utilized applies a weighting to more heavily use the rudder instead of the available rotor controls to maintain tip separation, as discussed in Refs. 24 and 25. Here, the tip clearance response is still large due to the presence of rotor controls in the allocation, but tip separation is maintained and the sideslip command is tracked well.

180 kt failure cases

All available actuators have a possibility of fault in all vehicle operating states. However, the present study considers only failure of the aerosurfaces (elevator and rudder) in the cruise condition. This approach is taken for brevity and also due to the fact that swashplate actuator failure appears at least notionally similar in hover and in cruise, with the difference being that undesired rotor hub force and moment can now be at least partially compensated for by the empennage surfaces instead of necessarily requiring differential moments in the rotor system.

Elevator fault is simulated by moving the surface from trim at -5° (trailing edge up) back to zero deflection at 5 s and locking it in place. This new setting introduces a transient response as expected, where the vehicle experiences a nose-down pitching moment and consequently a negative pitch rate (about -25 deg/s, or roughly -4 g load factor) and new trim pitch attitude at about nose level (Fig. 21). In order to compensate for the change in elevator setting, the rotor controls shift to rebalance vehicle vertical force and pitching moment to achieve $n_z = 1g$, indicated by the change in θ_0, θ_{lon}, and $\Delta\theta_{lat}$ in Fig. 22. This use of rotor head controls changes the rotor tip clearance as well, depicted in Fig. 23.

Rudder failure in a coaxial helicopter system is particularly challenging, due to the lack of efficient yawing moment generation from the dual rotor system in cruise. Granted, the rotor has enough control power to

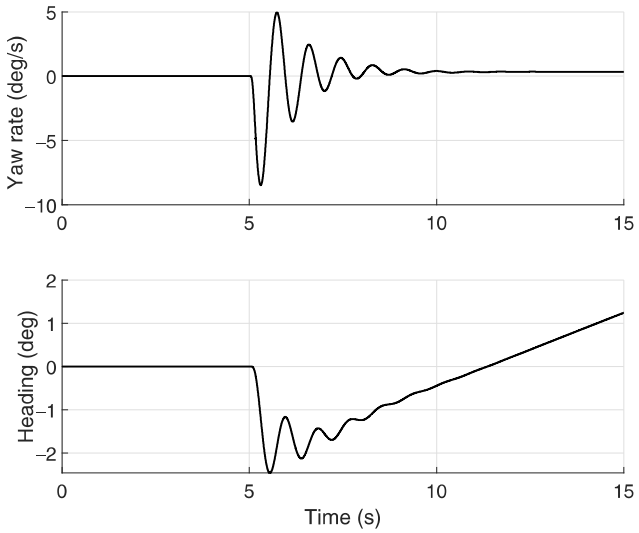

Fig. 24. Rudder failure yaw response, cruise.

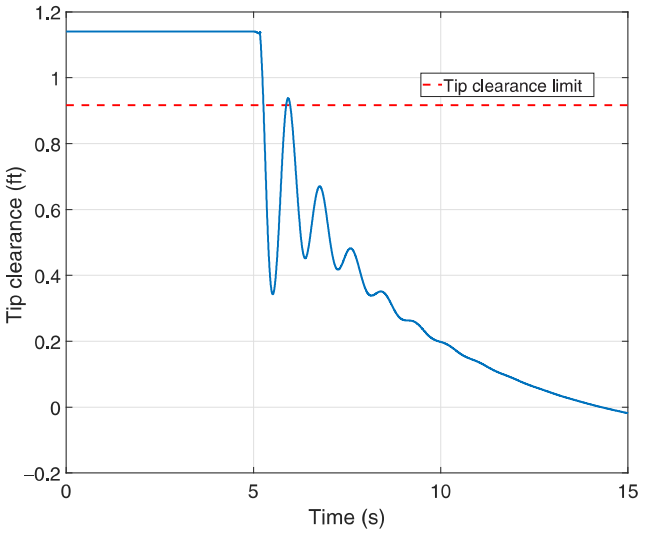

Fig. 26. Rudder failure tip clearance, cruise.

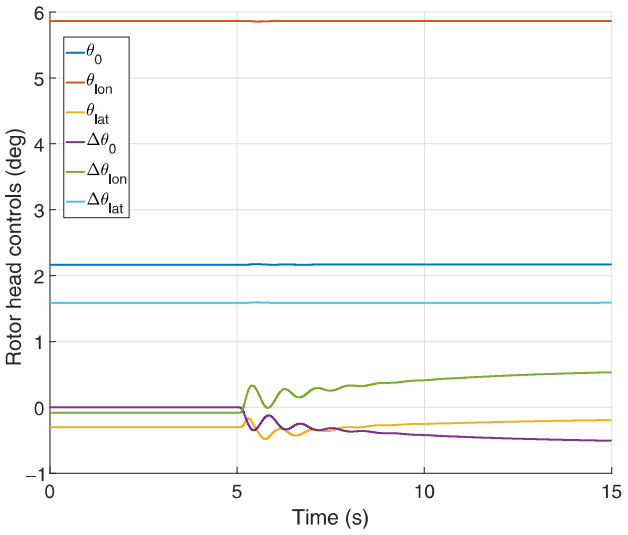

Fig. 25. Rudder failure rotor head controls, cruise.

generate any required moment for reasonable yaw rate or sideslip commands, but this requires the use of differential inputs to the rotor system. Differential inputs in general force the rotor into differential flapping states, which leads to reduction in tip clearance or even blade strike when large enough directional input is commanded.

To illustrate this problem, the rudder is moved and locked out of trim to a −5 deg position at 5 s simulation time. This new setting generates a nose-right yawing moment (Fig. 24), which requires the rotor to compensate using differential controls (Fig. 25).

As shown in Fig. 2, the primary controls that can be used to generate this net rotor hub torque are $\Delta\theta_0$, $\Delta\theta_{lon}$, and θ_{lat}, which are primarily differential moment generators, and so the rotor tip clearance is significantly impacted by this fault case (Fig. 26). Note that the total rudder range of deflection is $\pm 30^\circ$, so this locked position of 5° represents a fairly small deflection. Larger displacements of the rudder would in turn require larger compensation, at further detriment to the rotor tip clearance. This further illustrates the need for careful consideration of directional control authority on a coaxial helicopter platform; the addition of effectors such as propeller monocyclic may be required to ensure sufficient resilience to rudder failure.

Discussion and Conclusions

The presented results cover multiple operating states and fault conditions, presenting some of the specific information relevant to each case. Overall, some general discussion can be made on the system behavior in nominal and fault cases based on the included results.

Pseudoinverse control allocation was utilized to determine the optimal use of the redundant control effectors available on the coaxial helicopter in both hover and forward flight, using a weighted pseudoinverse approach, with weights defined by available actuator position limits. Different choices of weights in the pseudoinverse optimization can bias control effort as needed while retaining the vehicle acceleration achieved by the allocated modes. This was considered for the directional control channel in cruise, where biasing control toward the rudder resulted in rotor tip clearance improvement while maintaining the same command tracking performance.

Pseudoinverse control allocation allows for simple and fast recalculation of control mixing in the event of flight control failure. When failure occurs, the column of the B matrix used in Eq. (4) corresponding to the failed control is set to zero (to represent the lack of motion in the actuator when it locks), and the mixing is recalculated. This process effectively places infinite weight on the damaged control, ensuring that the allocation no longer commands any change in the failed flight control.

The recalculated pseudoinverse approach works well in terms of maintaining vehicle stability when failure occurs. In all fault cases considered, the aircraft recovers back to trim within 5 s of the failure with no additional pilot intervention required. In hover, the swashplate actuator failure considered represented a moderate displacement from the trim setting. As discussed in prior work by the authors (Ref. 19), the helicopter still possesses redundancy even in hover and can compensate for actuator failure in a single rotor by producing an opposite moment, resulting in a large lift offset and reduction in rotor tip clearance.

Cruise condition fault cases are simpler to account for in terms of the control reconfiguration, as there are more effectors available to the control system. In the present study, aerosurfaces are locked out of trim during steady flight, requiring the rotor system to compensate by providing large forces and moments to account for the new output of the tail surfaces.

Utilization of the rotor controls, especially at the high advance ratio, results in substantial tip clearance variation. In the event of rudder failure, a yawing moment must be produced by the rotor system alone, which requires a differential torque between the two rotors and a substantial reduction in the rotor tip clearance. This behavior is not easily avoided, and it may be necessary to include additional yaw controls like a propeller monocyclic or significantly reduce the allowable pilot commands in the directional control channel.

Because rotor tip clearance is a key safety parameter during the operation of a coaxial helicopter, control design should take impact on rotor tip clearance into account. The present study does not investigate the implementation of a tip clearance controller, but work done at the U.S. Army has considered a tip clearance controller in the forward path control (Ref. 11). This would aid in the healthy cases presented here, but the benefit from use of a tip clearance controller in a failure state is unclear, particularly in a swashplate actuator fault state. Again, the directional control of the vehicle appears to be the most critical for consideration, and items should be considered in future study.

Acknowledgments

This work was carried out at the Rensselaer Polytechnic Institute under the Army/Navy/NASA Vertical Lift Research Center of Excellence (VLRCOE) Program, grant number W911W61120012, with Dr. Mahendra Bhagwat as a Technical Monitor. The authors would also like to acknowledge the Department of Defense and the Army Research Office for sponsoring Dr. McKay through the National Defense Science and Engineering Graduate Fellowship.

References

[1]Colucci, F., "The Moving Parts of Future Vertical Lift," *Vertiflite Magazine*, Vol. 65, (5), September/October 2019, pp. 12–16.

[2]Jacobellis, G., Gandhi, F., and Floros, M., "Using Control Redundancy for Power and Vibration Reduction on a Coaxial Rotor Helicopter at High Speeds," *Journal of the American Helicopter Society*, **64**, 032008 (2019), DOI: 10.4050/JAHS.64.032008.

[3]Reddinger, J.P., Gandhi, F., and Kang, H., "Using Control Redundancy for Power and Vibration Reduction on a Compound Helicopter at High Speeds," *Journal of the American Helicopter Society*, **63**, 032009 (2018), DOI: 10.4050/JAHS.63.032009.

[4]Reddinger, J.P., and Gandhi, F., "Physics-Based Trim Optimization of an Articulated Slowed-Rotor Compound Helicopter in High-Speed Flight," *Journal of Aircraft*, 52, (6), December 2015, pp. 1756–1766, DOI: 10.2514/1.C032939.

[5]Herrmann, T., Celi, R., and Baeder, J., "Multidisciplinary Trim Analysis of a Coaxial-Pusher Rotorcraft Configuration," Proceedings of the 74th Annual Forum of the Vertical Flight Society, Phoenix, AZ, May May 14–17, 2018.

[6]Herrmann, T., Celi, R., and Baeder, J., "Multidisciplinary, Multiobjective Trim Optimization for a Coaxial-Pusher Rotorcraft Configuration," Proceedings of the 75th Annual Forum of the Vertical Flight Society, Philadelphia, PA, May 13–16, 2019.

[7]Herrmann, T., Celi, R., and Baeder, J., "Multidisciplinary Trim Analysis Using Improved Optimization, Image Analysis, and Machine Learning Algorithms," Proceedings of the 77th Annual Forum of the Vertical Flight Society, Virtual, May 10–14, 2021.

[8]Berger, T., Juhasz, O., Lopez, M. J. S., Tischler, M. B., and Horn, J. F., "Modeling and Control of Lift Offset Coaxial and Tiltrotor Rotorcraft," *CEAS Aeronautical Journal*, 11, (1), January 2020, pp. 191–215, DOI: 10.1007/s13272-019-00414-0.

[9]Fegely, C., Juhasz, O., Xin, H., and Tischler, M.B., "Flight Dynamics and Control Modeling with System Identification Validation of the Sikorsky X2 Technology Demonstrator," Proceedings of the 72nd Annual Forum of the American Helicopter Society, West Palm Beach, FL, 17–19, May 2016.

[10]Juhasz, O., Xin, H., and Tischler, M. B., "Inflow Based Flight Dynamics Modeling Improvements for the Sikorsky X2 Technology™ Demonstrator," Proceedings of the 76th Annual Forum of the Vertical Flight Society, Virtual, October 5–8, 2020.

[11]Berger, T., Blanken, C. L., Tischler, M. B., and Horn, J. F., "Flight Control Design and Simulation Handling Qualities Assessment of High-Speed Rotorcraft," Proceedings of the 75th Annual Forum of the Vertical Flight Society, Philadelphia, PA, May 13–16, 2019.

[12]Berger, T., Tischler, M. B., and Horn, J. F., "Outer-Loop Control Design and Simulation Handling Qualities Assessment for a Coaxial-Compound Helicopter and Tiltrotor," Proceedings of the 76th Annual Forum of the Vertical Flight Society, Virtual, October 5–8, 2020.

[13]Reddinger, J.P., and Gandhi, F., "Using Redundant Effectors to Trim a Compound Helicopter with Damaged Main Rotor Controls," Proceedings of the 73rd Annual Forum of the American Helicopter Society, Fort Worth, TX, May 9–11, 2017.

[14]Vayalali, P., McKay, M., and Gandhi, F., "Redistributed Pseudoinverse Control Allocation for Actuator Failure on a Compound Helicopter," Proceedings of the 76th Annual Forum of the Vertical Flight Society, Virtual, October 5–8, 2020.

[15]Vayalali, P., McKay, M., and Gandhi, F., "Fault-Tolerant Control Allocation on a Compound Helicopter in Cruise," Proceedings of the 77th Annual Forum of the Vertical Flight Society, Virtual, May 10–14, 2021.

[16]Vayalali, P., McKay, M., Krishnamurthi, J., and Gandhi, F., "Horizontal Stabilator Utilization for Post Swashplate Failure Operation on a UH-60 Black Hawk Helicopter," *Journal of the American Helicopter Society*, **65**, 022009 (2019), DOI: 10.4050/JAHS.65.022009.

[17]Vayalali, P., McKay, M., Krishnamurthi, J., and Gandhi, F., "Fault-Tolerant Control on a UH-60 Black Hawk Helicopter Using Horizontal Stabilator," *CEAS Aeronautical Journal*, 12, (1), January 2021, pp. 13–27, DOI: 10.1007/s13272-020-00476-5.

[18]Knapp, M. E., Ivler, C. M., Horn, J. F., Johnson, E. N., Bridges, D. O., Lopez, M. J. S., Tischler, M. B., Wagster, J. A., and Cheung, K. K., "Development and Simulation of Damage Tolerant Control Laws for a Compound Helicopter," Proceedings of the AIAA SciTech 2020 Forum, Orlando, FL, January 6–10, 2020.

[19]McKay, M., Vayalali, P., and Gandhi, F., "Post-Failure Control Reconfiguration on a High-Speed Lift-Offset Coaxial Helicopter," Proceedings of the 76th Annual Forum of the Vertical Flight Society, Virtual, October 5–8, 2020.

[20]Kong, Y. B., Prasad, J. V. R., and Peters, D., "Development of a Finite State Dynamic Inflow Model for Coaxial Rotor using Analytical Methods," Proceedings of the 73rd Annual Forum of the American Helicopter Society, Fort Worth, TX, May 9–11, 2017.

[21]Harrington, R. D., "Full-Scale-Tunnel Investigation of the Static-Thrust Performance of a Coaxial Helicopter Rotor," NACA TR 2318, March 1951.

[22]Feil, R., Raulder, J., Cameron, C., and Sirohi, J., "Aeromechanics Analysis of a High Advance Ratio Lift Offset Coaxial Rotor System," *Journal of Aircraft*, 56, (1), 2019, pp. 166–178, DOI: 10.2514/1.C034748.

[23]Ferguson, S. W., "A Mathematical Model for Real Time Flight Simulation of a Generic Tilt-Rotor Aircraft," NASA CR 166539, September 1988.

[24]McKay, M. E., "Fault Tolerant Control of Multirotor Vehicles," Ph.D. Thesis, Rensselaer Polytechnic Institute, Troy, NY, November 2021.

[25]McKay, M., Vayalali, P., Gandhi, F., Berger, T., and Lopez, M. J. S, "Redistributed Allocation for Flight Control Failure on a Coaxial Helicopter," Proceedings of the 77th Annual Forum of the Vertical Flight Society, Virtual, May 10–14, 2021.

[26]Tischler, M., Berger, T., Ivler, C., Mansur, M., Cheung, K., and Soong, J., *Practical Methods for Aircraft and Rotorcraft Flight Control Design: An Optimization-Based Approach*, AIAA Education Series, AIAA, Reston, VA, 2017.

[27]Ivler, C. M., and Juhasz, O., "Evaluation of Control Allocation Techniques for Medium Lift Tilt-Rotor," Proceedings of the 71st Annual Forum of the American Helicopter Society, Virginia Beach, VA, May 5–7, 2015.

[28]Enns, D., "Control Allocation Approaches," AIAA Guidance, Navigation, and Control Conference and Exhibit, Boston, MA, August 10–12, 1998.

[29]Tischler, M., and Remple, R., *Aircraft and Rotorcraft System Identification: Engineering Methods with Flight Test Examples*, AIAA Education Series, AIAA, Reston, VA, 2006.

[30]"Handling Qualities Requirements for Military Rotorcraft," Aeronautical Design Standard and Performance, Specification (ADS-33E-PRF), U.S. Army Aviation and Missile Command, 2000.

[31]Walsh, D., Weiner, S., Arifian, K., Lawrence, T., Wilson, M., Millott, T., and Blackwell, R., "High Airspeed Testing of the Sikorsky X2 Technology Demonstrator," Proceedings of the 67th Annual Forum of the American Helicopter Society, Virginia Beach, VA, May 3–5, 2011.